General Disclaimer

One or more of the Following Statements may affect this Document

- This document has been reproduced from the best copy furnished by the organizational source. It is being released in the interest of making available as much information as possible.

- This document may contain data, which exceeds the sheet parameters. It was furnished in this condition by the organizational source and is the best copy available.

- This document may contain tone-on-tone or color graphs, charts and/or pictures, which have been reproduced in black and white.

- This document is paginated as submitted by the original source.

- Portions of this document are not fully legible due to the historical nature of some of the material. However, it is the best reproduction available from the original submission.

EOSL

Electro-Optics Systems Laboratory
Department of Electrical and Computer Engineering

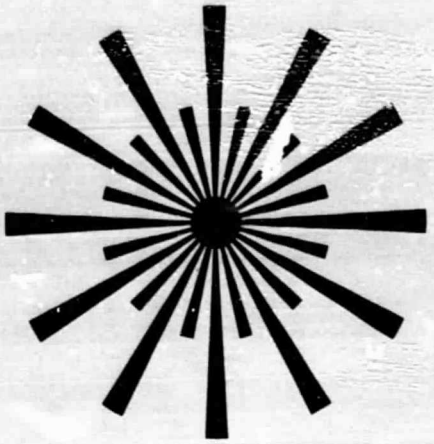

Phase-Locked Loop Synchronization for Direct Detection Optical PPM Communication Systems

Chien C. Chen • C. S. Gardner

EOSL No. 85-003 • May 1985

University of Illinois at Urbana-Champaign

UILU-ENG-85-2549

PHASE LOCKED LOOP SYNCHRONIZATION FOR DIRECT DETECTION OPTICAL PPM COMMUNICATION SYSTEMS

by

C. C. Chen
C. S. Gardner

EOSL Publication No. 85-003

Technical Report
May 1985

Supported by
Contract No. NASA NSG-5049

NATIONAL AERONAUTICS & SPACE ADMINISTRATION
Goddard Space Flight Center
Greenbelt, Maryland 20771

ELECTRO-OPTIC SYSTEMS LABORATORY
DEPARTMENT OF ELECTRICAL AND COMPUTER ENGINEERING
COLLEGE OF ENGINEERING
UNIVERSITY OF ILLINOIS
URBANA, ILLINOIS 61801

ABSTRACT

Receiver timing synchronization of an optical PPM communication system can be achieved using a phase-locked loop (PLL) if the photodetector output is properly processed. The synchronization performance is shown to improve with increasing signal power and decreasing loop bandwidth. Bit error rate (BER) of the PLL synchronized PPM system is analyzed and compared to that for the perfectly synchronized system. It is shown that the increase in signal power needed to compensate for the imperfect synchronization is small (less than 0.1 dB) for loop bandwidths less than 0.1 % of the slot frequency.

TABLE OF CONTENTS

1. INTRODUCTION

M-ary Pulse Position Modulation (M-PPM) has been shown to be an effective modulation technique for direct detection optical communications. In M-ary PPM systems, each word frame is divided into M time slots and the data are encoded by transmitting a single laser pulse during one of the M time slots. The performance of optical PPM systems has been well documented [1,2,3]. However, most studies were based on the assumption of perfect timing synchronization between the receiver and the transmitter. For a practical communication system, this condition is not always satisfied.

In the presence of timing error, some of the signal photons that are transmitted in the signal time slot will be counted in the adjacent slots. This effectively reduces the signal-to-noise ratio and, consequently, increases the probability of decoding error [3]. Accurate timing synchronization is needed to minimize the decoding error at the receiver. In general, timing synchronization can be achieved by either transmitting a separate timing signal along with the data, or by acquiring synchronization directly from the received signal. For applications where the transmitter power is limited, the latter method is preferred. Phase-locked loops (PLLs) provide an easily implemented method for recovering the transmitter timing. The applications of phase-locked loops in radio frequency systems have been studied extensively [4,5]. The use of phase-locked loops for timing synchronization in optical communication systems have also been studied in recent years [6,7,8]. Gagliardi and Haney [6] and Snyder and Porrester [7] analyzed the probability density of tracking error for a PLL under shot noise input. Mengali and Pezzani [8] studied the phase error variance of a PLL driven by photodetector current in an optical pulse amplitude modulation

(PAM) system. These studies have shown that that PLLs can be used to track the transmitter timing provided that the transmitted signal contains a frequency component at the desired lock-in frequency. In related work, Georghiades [9] and Georghiades and Snyder [10] studied the problem of obtaining frame and word synchronizations of a PPM system using a coding technique, with the assumption that slot synchronization has been achieved.

In this paper, it is shown that for a PPM system which transmits square pulses occupying the entire signal slot, phase-locked loops cannot lock onto the photodetector output directly because the detected signal does not contain a spectral component at the time slot frequency. However, with proper preprocessing of the photodetector output, namely, squaring the detected signal, PLLs can be used to lock onto the transmitter slot frequency. The performance of the PLL using the preprocessed PPM signal is then analyzed using a perturbation method [8], and an expression for phase error variance is derived. Finally, the error performances of phase-locked loop synchronized PPM systems are evaluated and compared with perfectly synchronized systems.

2. SIGNAL AND NOISE AT THE PHOTODETECTOR OUTPUT

The output current of the photodetector can be modeled as the sum of a signal shot noise and a Gaussian thermal noise. Furthermore, the signal shot noise can be modeled as a filtered point process in which the output is the superposition of the detector response to each detected photon [11]. The detector output can be written as

$$i(t) = i_s(t) + i_{th}(t) = \sum_{\{\tau_j\}} G \cdot h(t - \tau_j) + i_{th}(t) \qquad (1)$$

where $i_s(t)$ and $i_{th}(t)$ are the signal shot noise and the thermal noise current, respectively, $h(t)$ is the combined pulse response of the detector and subsequent amplifier-filters, G is the photodetector gain (assumed to be constant), and τ_j is the arrival time of the j^{th} photon. For simplicity, it is assumed that the internal gain of the photodetector is large so that the effects of the thermal noise can be neglected. The principal source of noise at the detector output is therefore the signal shot noise, which is due to the stochastic nature of the photon counting process.

The photocount statistics at the photodetector, conditioned on the received optical power, can be shown to be Poisson distributed with count rate $\lambda(t)$, which is related to the received optical power [2].

$$\lambda(t) = \eta P_o(t)/h\nu_o \quad . \qquad (2)$$

η is the quantum efficiency of the detector, $P_o(t)$ is the total received power at the detector surface and $h\nu_o$ is the photon energy. The total optical power incident on the detector surface is the sum of the received signal power and

the power of the background radiation. The photocount rate $\lambda(t)$ is therefore the sum of the background rate and the count rate due to the signal. For an M-ary PPM system, the photocount rate can be modeled as

$$\lambda(t) = \lambda_b + \sum_k \lambda_s \, p(t - kT_w - C_k T_s) \tag{3}$$

where λ_s is the photocount rate due to the signal, λ_b is the constant photocount rate due to the uniform background radiation, T_w is the word frame period, T_s is the time slot width, which equals T_w/M, C_k is the k^{th} codeword which takes on the integer values $(0,1,\ldots,M-1)$, and $p(t)$ is a unit square pulse of width T_s.

Since the transmitted data $\{C_k\}$ are random, $\lambda(t)$ is a stochastic process. The output of the photodetector can therefore be regarded as a sample function of a doubly stochastic filtered Poisson process [12]. The statistics of this process can be evaluated by first taking the expectation conditioned on the received photocount rate $\lambda(t)$, using the fact that the conditioned process is a filtered Poisson process. This conditioning can then be removed by taking the expectation with respect to the transmitted data. The expectations of the filtered Poisson process can be obtained by differentiating its characteristic function [12], given by

$$\begin{aligned} \Phi(\omega) &= E[e^{-j\omega i_s(t)}] \\ &= \exp[\int \lambda(\xi)(e^{-j\omega h(t-\xi)} - 1)d\xi] \quad . \end{aligned} \tag{4}$$

The first and second moments of the detector output, conditioned on the detector photocount rate, are given by

$$E[i(t)|\lambda] = G\lambda(t)*h(t) \tag{5}$$

$$E[i^2(t)|\lambda] = G^2[\lambda(t)*h^2(t) + (\lambda(t)*h(t))^2] \quad . \tag{6}$$

The unconditioned moments of the detector output can be obtained by taking the expectations of Equations (5) and (6) with respect to the data $\{C_k\}$. If $\{C_k\}$ are independent and uniformly distributed, the resulting unconditioned moments of the detector output are given by

$$E[i(t)] = G\left(\lambda_b + \frac{\lambda_s}{M}\sum_{\ell=-\infty}^{\infty} p(t - \ell T_s)\right)*h(t) \tag{7}$$

$$\begin{aligned} E[i^2(t)] = G^2\Bigg(&\left(\lambda_b + \frac{\lambda_s}{M}\sum_{\ell=-\infty}^{\infty} p(t - \ell T_s)\right)*h^2(t) + \left[\left(\lambda_b + \frac{\lambda_s}{M}\sum_{\ell=-\infty}^{\infty} p(t - \ell T_s)\right)*h(t)\right]^2 \\ &+ \frac{1}{M}\lambda_s^2 \sum_{\ell=-\infty}^{\infty}[h(t)*p(t - \ell T_s)]^2 - \frac{1}{M^2}\sum_{k=-\infty}^{\infty}\sum_{\substack{\mu=0\\ \nu=0}}^{M-1} h(t)*p(t - kT_w - \nu T_s) \\ &\times h(t)*p(t - kT_w - \mu T_s)\Bigg] \end{aligned} \tag{8}$$

where $p(t)*h(t)$ denotes the convolution of $p(t)$ and $h(t)$. Notice that by taking the expectation with respect to the transmitted data, the expected moments of the detector output now contain periodic terms with period T_s. Phase-locked loops can then be used to lock onto these signals and generate timing references.

3. SIGNAL PREPROCESSING

In an optical M-ary PPM signaling system that transmits equally likely codewords, the optimal receiver [1,2] compares the received photocount in each of the M time slots and chooses the time slot with the largest photocount. This decoding operation cannot be achieved without timing synchronization between the receiver and the transmitter. For this reason, it is important for the receiver to maintain a local timing reference which identifies the beginning of each transmitted time slot. With proper preprocessing, phase-locked loops can be used to generate this local timing reference from the photodetector output.

A block diagram of a typical phase-locked loop [4,5] is shown in Figure 1. It consists of a voltage controlled oscillator (VCO), a low pass filter and a phase detector, which generates an output voltage as a function of the phase difference between the VCO output and the incoming signal. In order to achieve effective phase synchronization, the input signal to the PLL must contain a strong periodic component at the lock-in frequency.

From Equation (7), it is seen that if the transmitted pulse p(t) is a square pulse of width T_s, the expected output of the photodetector is a constant

$$E[i(t)] = (\lambda_b + \frac{\lambda_s}{M}) * h(t) = (\lambda_b + \frac{\lambda_s}{M}) \cdot \int_{-\infty}^{\infty} h(\tau) d\tau \quad . \tag{9}$$

Therefore, the detector output does not contain a periodic component at the slot frequency. This fact is also seen by examining the signal power spectrum. Based on the model of the photodetector output given in Equation (1), the power spectrum of the detector output for an M-ary PPM receiver can be shown to be (Appendix A):

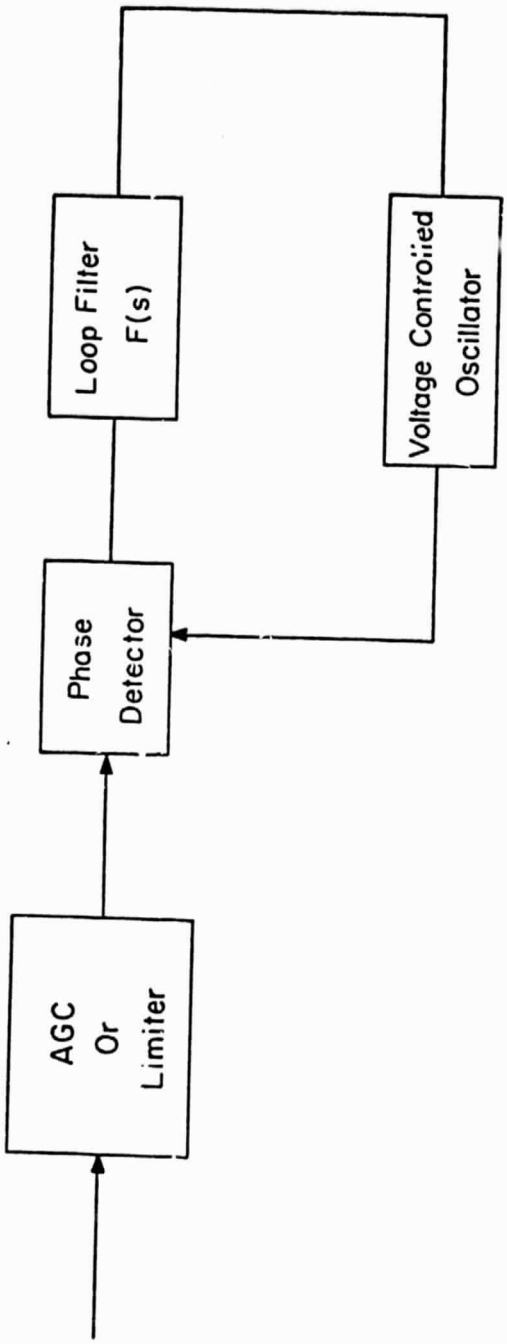

Figure 1. Block diagram of a phase locked loop.

$$S(\omega) = G^2 \cdot |H(\omega)|^2 \cdot \left[(\lambda_b + \frac{\lambda_s}{M}) + 2\pi\delta(\omega)(\lambda_b^2 + \frac{2\lambda_s\lambda_b}{M}) \right.$$

$$\left. + \frac{\lambda_s^2}{T_w} |p(\omega)|^2 (1 - |R(\omega)|^2) + \frac{2\pi}{T_w} \lambda_s^2 |p(\omega)|^2 \cdot \sum_{k=-\infty}^{\infty} \delta(\omega - \frac{2\pi k}{T_s}) \right] \quad (10)$$

where

$$R(\omega) = E[\exp(-jC_k \omega T_s)] = \frac{1}{M} \sum_{\ell=0}^{M-1} e^{-j\omega\ell T_s} \quad (11)$$

and $P(\omega)$ and $H(\omega)$ denote the Fourier transforms of the pulse shape and the impulse response of the detector-filter, respectively. If the transmitted pulse shape is a square pulse with width T_s, its Fourier transform $P(\omega)$ will be zero at all integer multiples of the slot frequency, $2\pi/T_s$. In this case, it is seen from Equation (10) that no discrete frequency components at the slot frequency or its harmonics exist in the detector output spectrum. Consequently, the phase-locked loop cannot track the output of the photodetector directly. Preprocessing of the detector output is necessary to generate a frequency component at the slot frequency.

Only nonlinear processing needs to be considered, because any linear filtering will simply amount to multiplying the power spectrum in Equation (10) by the magnitude square of the filter transfer function, and will not affect the absence of the spectral component at the slot frequency. One approach is to filter the signal and then square the filter output, as depicted in Figure 2. The output of this preprocessing circuit can be written as

$$i_2(t) = i^2(t) = \left[\sum_{\{\tau_j\}} G \cdot h(t - \tau_j) \right]^2 \quad (12)$$

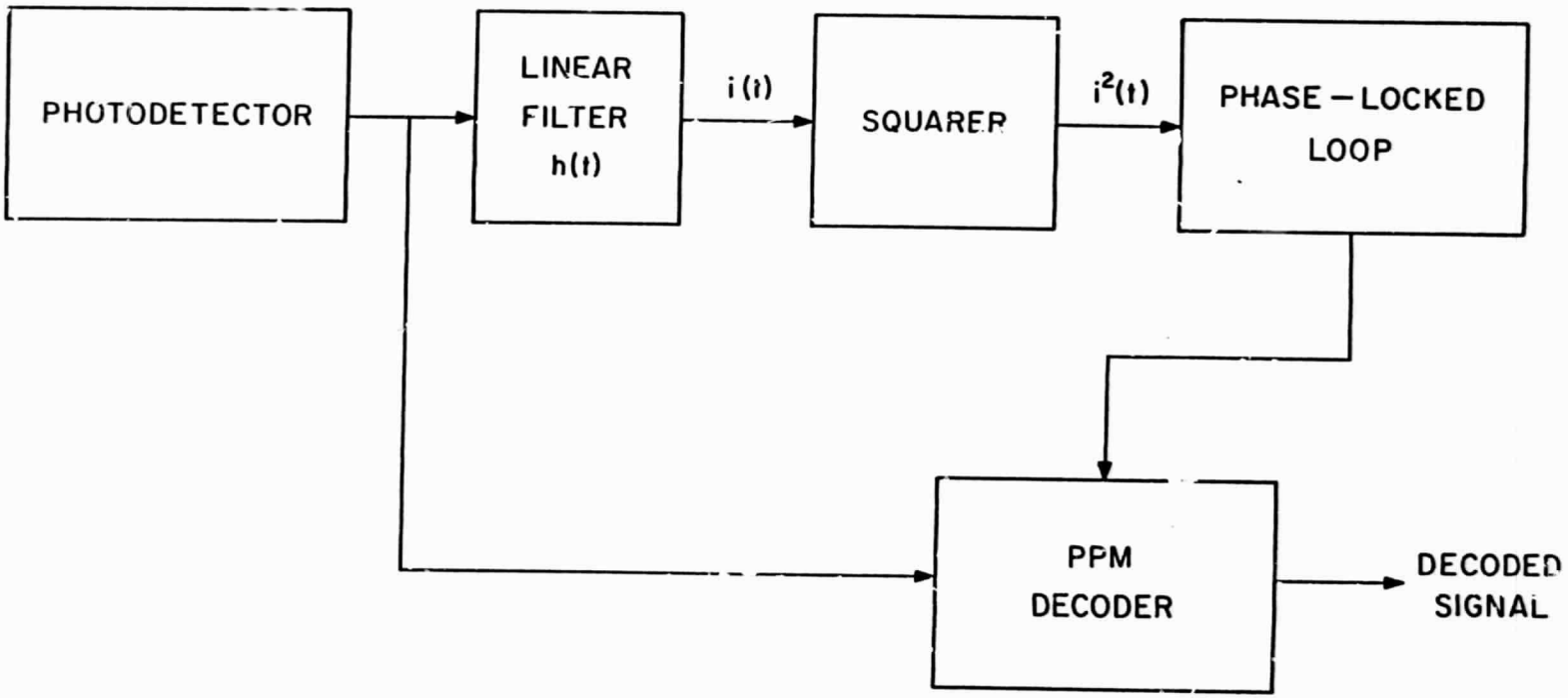

Figure 2. The structure of the receiver timing subsection. The output of the photodetector is first filtered by a preprocessing filter before being squared. The output of the squarer is then fed into the PLL to generate the local timing reference.

where h(t) now denotes the combined impulse response of the detector and the preprocessing filter. The expected output of this preprocessing circuit is given by Equation (8). By examining Equation (8), it is seen that the third term at the right-handed side is periodic with period T_s and, unlike the photodetector output, does not have a vanishing Fourier transform at the slot frequency. The output of the preprocessing circuit can therefore be regarded as the sum of a periodic signal s(t) and an additive noise term n(t), related by

$$i_2(t) = s(t) + n(t) \tag{13}$$

where from Equation (8)

$$s(t) = G^2 \frac{\lambda_s^2}{M} \sum_{\ell=-\infty}^{\infty} [p(t)*h(t - \ell T_s)]^2$$

$$n(t) \triangleq i_2(t) - s(t) \quad . \tag{14}$$

The power spectrum of the preprocessed signal is quite complicated. However, the expression for the power spectrum can be simplified considerably if it is assumed that $H(\omega)$ blocks the dc component of the signal, and that both $P(\omega)$ and $H(\omega)$, the Fourier transforms of p(t) and h(t), are slowly varying functions of frequency compared to $R(\omega)$, defined in Equation (11). The first assumption is made because the dc component of the detector output contains no timing information and will only contribute noise to the squared signal. Therefore, it is desirable to remove the dc component from the photodetector output. The second assumption holds for higher-order PPMs. Because, in general, h(t) and p(t) are pulses of width comparable to T_s, their Fourier transforms will have supports on the order of $\omega_s = 2\pi/T_s$. The support for $R(\omega)$, on the other hand, is on the

order of ω_s/M, where M is the PPM order. Therefore, for high-order PPM, the assumption that $P(\omega)$ and $H(\omega)$ are slowly varying compared to $R(\omega)$ usually holds. For high signal counts, the power spectrum of the preprocessed signal $i_2(t)$ near the slot frequency can be approximated under these assumptions by (Appendix B)

$$S_2(\omega) = S_s(\omega) + S_n(\omega) \tag{15}$$

where

$$S_s(\omega) = \frac{\lambda_s^4}{T_w^2} G^4 \cdot \frac{1}{2\pi} \left| P(\omega)H(\omega) * P(\omega)H(\omega) \right|^2 \cdot \delta(\omega - \omega_s) \tag{16}$$

$$S_n(\omega) = 4 \frac{\lambda_s^3}{T_w} G^4 \cdot \frac{1}{(2\pi)^2} \int P(\omega')P^*(\omega'')P^*(\omega' - \omega'')H(\omega')H(\omega - \omega')H^*(\omega'') \times H^*(\omega - \omega'')d\omega'd\omega'' \quad . \tag{17}$$

The power spectrum of the preprocessed photodetector output can be separated into two terms. $S_s(\omega)$ is due to the sinusoidal signal component s(t) in the preprocessed signal, and $S_n(\omega)$ is the power spectrum of the additive noise, n(t), which is the random component of the preprocessor output. From Equation (16), s(t) can be written as

$$s(t) = A \sin(\omega_s t + \theta_s)$$

$$A = \frac{2\lambda_s^2 G^2}{T_w} \left| \frac{1}{2\pi} \int P(\omega')H(\omega')P(\omega_s - \omega')H(\omega_s - \omega')d\omega' \right| \tag{18}$$

where $\omega_s = 2\pi/T_s$ is the frequency of the sinusoid, which is equal to the slot frequency, and A and θ_s are the amplitude and phase, respectively.

4. PLL ANALYSIS

The presence of the sinusoidal component with slot frequency at the preprocessor output indicates that PLL can now be used to track the transmitting timing. The PPL depicted in Figure 1 has the equivalent baseband model shown in Figure 3 [4,5]. In reducing the PLL to its baseband model, it is assumed that the input consists of a sinusoidal signal s(t) with frequency ω_s and amplitude A, and an additive noise term n(t), and that the VCO has gain constant K_v and free-running frequency ω_0, which differs from ω_s by an amount Ω, the frequency detuning. From the baseband model, it is straightforward to show that the phase error ϕ between the VCO output and the incoming sinusoid satisfies

$$\frac{d\phi}{dt} = \Omega - K_v f(t) * [\frac{A}{2} \sin\phi + n(t) \cos(\omega_s t + \theta_s - \phi)] \tag{19}$$

where f(t) is the impulse response of the loop filter, and θ_s is the initial phase of the incoming signal. In general, Equation (19) is a stochastic integro-differential equation that is difficult to solve. However, if the noise term n(t) is small, we can make a perturbation expansion of Equation (19) [8]. The result, after expansion, is a series of equations that can be solved recursively. The first two terms of the expansion satisfy the equations

$$\frac{d\phi_0}{dt} = \Omega - \frac{A}{2} K_v f(t) * \sin\phi_0 \tag{20}$$

$$\frac{d\phi_1}{dt} = -K_v f(t) * (\frac{A}{2}\phi_1 \cos\phi_0 + n(t)\cos(\omega_s t + \theta_s - \phi_0)) \quad . \tag{21}$$

The phase error at the VCO output can then be approximated by

$$\phi(t) \simeq \phi_0(t) + \phi_1(t) \quad . \tag{22}$$

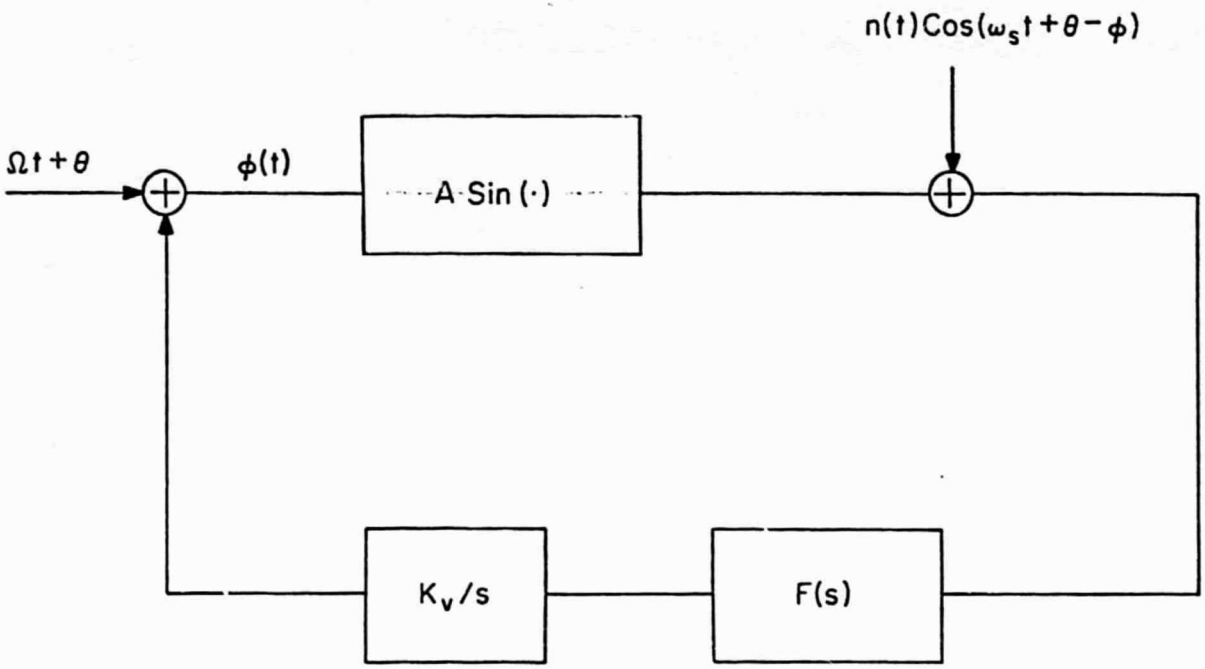

$$\frac{d\phi}{dt} = \Omega - KF(p)\left\{ A \sin\phi + n(t)\cos(\omega_s t + \theta - \phi)\right\}$$

Figure 3. Baseband model of the phase-locked loop.

The solution of Equation (20) gives the phase error as a function of time when no noise appears at the input. In the steady state, ϕ_0 tends to

$$\phi_0(\infty) \simeq \sin^{-1}\left(\frac{\Omega}{\frac{A}{2} KF(0)}\right) \tag{23}$$

where F(s) is the transfer function of the loop filter, which is related to the impulse response f(t) by a Laplace transform. When noise is present at the input to the PLL, higher-order solutions to the phase error must be included to account for the noise effects. The first-order equation, Equation (21), contains a stochastic driving term n(t) on the right-hand side. Consequently, its solution will also be stochastic. In the steady state, the solution to Equation (21) is given by

$$\phi_1(t) \simeq \frac{2}{A} g(t) * [n(t)\cos(\omega_s t + \theta_s - \phi_0)] \tag{24}$$

where g(t) is the inverse Laplace transform of the loop transfer function G(s) defined as

$$G(s) = \frac{A}{2} KF(s) / \left(s + \frac{A}{2} KF(s)\cos\phi_0\right) \quad . \tag{25}$$

Equation (24) states that the first-order solution of the phase error is the filtered output of the stochastic driving term

$$\nu(t) = n(t)\cos(\omega_s t + \theta_s - \phi_0) \quad . \tag{26}$$

The autocorrelation function of the phase error $R_\phi(t,\tau)$ can therefore be related to the autocorrelation of the process $\nu(t)$ by

$$R_\phi(t,\tau) = R_\nu(t,\tau) * g(t) * g(\tau) \tag{27}$$

from which the variance of phase error can be calculated. In general, $\phi(t)$ is not stationary. In fact, it can be shown that for PPM transmission, n(t), and consequently $\nu(t)$, are cyclostationary with period T_w. It follows that the variance of phase error σ_ϕ^2 is also periodic with period T_w.

However, when the loop bandwidth is small, it is found that ϕ is actually a wide sense stationary (WSS) process [13]. More specifically, ϕ is WSS if the loop transfer function satisfies

$$|G(\omega)| = 0 \text{ for } \omega > \frac{\pi}{T_w} = \frac{\omega_s}{2M} \tag{28}$$

In this case, the variance of ϕ can be written as

$$\sigma_\phi^2 = \frac{1}{2\pi}\frac{4}{A^2}\int |G(\omega)|^2 \cdot S_{\tilde{\nu}}(\omega)d\omega \tag{29}$$

where $S_{\tilde{\nu}}(\omega)$ is the power spectral density of the WSS process $\tilde{\nu}(t)$ derived from $\nu(t)$ by randomizing its initial phase, i.e., letting $\tilde{\nu}(t) = \nu(t + x)$ with x, the initial phase, to be uniformly distributed over $(0,T_w)$. In practice, for the PLL to have a sufficiently small phase error, the loop bandwidth should be much smaller than the time slot frequency. Consequently, Equation (28) is almost always satisfied.

The power spectrum $S_{\tilde{\nu}}(\omega)$ can be evaluated in terms of the noise power spectrum, which yields

$$S_{\tilde{\nu}}(\omega) = \frac{1}{4}\left(S_n(\omega + \omega_s) + S_n(\omega - \omega_s)\right)$$

$$+ \lim_{T\to\infty}\frac{1}{2T}\int_{-\infty}^{\infty} e^{-j\omega\tau}\int_{-T}^{T} R_n(t,t+\tau)\cos\left(\omega_s(2t+\tau) + 2\theta_s - \phi_0\right)dtd\tau \tag{30}$$

where $S_L(\omega)$ and $R_n(t,\tau)$ are the time-averaged power spectrum (Appendix A) and the autocorrelation function of the noise, respectively. For the PPM signaling scheme, the last term in Equation (30) is negligible compared to the first two terms. The variance of phase error in Equation (29) can then be written as

$$\sigma_\phi^2 = \frac{1}{A^2}\frac{1}{2\pi}\int |G(\omega)|^2 \left(S_n(\omega + \omega_s) + S_n(\omega - \omega_s)\right)d\omega. \tag{31}$$

Equation (31) can be further simplified if the bandwidth of the loop transfer function is sufficiently small so that $S_n(\omega)$ is approximately constant over the support of $G(\omega)$. Using the fact that $S_n(-\omega) = S_n(\omega)$, Equation (31) can be approximated by

$$\sigma_\phi^2 \simeq \frac{B_L}{A^2\pi} S_n(\omega_s) = \frac{1}{\rho} \tag{32}$$

where $\rho = A^2\pi/\left(S_n(\omega_s)B_L\right)$ can be interpreted as the signal-to-noise ratio of the synchronization signal within the effective loop bandwidth B_L (radians/second), defined as

$$B_L \triangleq \int_{-\infty}^{\infty} |G(\omega)|^2 d\omega. \tag{33}$$

By substituting the expression for noise power spectrum from Equation (17) and the expression for signal amplitude from Equation (18) into Equation (32), the following expression for the variance of phase error is obtained:

$$\sigma_\phi^2 = \frac{M}{K_s}\left(\frac{B_L}{\omega_s}\right)\gamma \tag{34}$$

$$\gamma = \left[\frac{2T_s \iint P(\omega')P^*(\omega'')P^*(\omega' - \omega'')H(\omega - \omega')H^*(\omega'')H^*(\omega - \omega'')d\omega' d\omega''}{|P(\omega)H(\omega) * P(\omega)H(\omega)|^2}\right]_{\omega = \omega_s}$$

where K_s is the signal count per word, M is the order of the PPM, B_L is the equivalent loop bandwidth, ω_s is the slot frequency, and γ is a dimensionless parameter, which depends only on the pulse shape and the preprocessing filter transfer function. The values of γ for some choices of preprocessing filter transfer functions are listed in Table 1. For a given pulse shape, the transfer function of the preprocessing filter can be chosen to minimize the value of γ. One choice is to model $H(\omega)$ as an ideal low pass differentiator with bandwidth B_0. Figure 4 is a plot of the value of γ versus the bandwidth of the differentiator for the case where $p(t)$ is a square pulse of width T_s. It is shown that the value of γ is minimized ($\gamma \approx 3.2$) for $B_0 \approx 1.3\omega_s$. Also shown in Figure 4 is the value of γ evaluated using the preprocessing filter which consists of a low pass Gaussian filter with rms bandwidth B_0, followed by an ideal differentiator. It is seen that the minimum values of γ obtained using both preprocessing filters are similar.

Equation (34) shows that variance of the phase error is inversely proportional to the signal power (i.e., signal photocount K_s) and is proportional to the number of time slots M and the loop bandwidth. It should be noted that the loop bandwidth B_L, defined in Equation (33), actually increases with increasing signal amplitude. In order to accommodate a wide dynamic range of input signals, it is the usual practice to precede the PLL by either an automatic gain control (AGC) circuit or a limiter. The effect of the AGC or limiter is to dynamically scale the input signal so that its amplitude remains essentially constant and, therefore, the loop bandwidth also remains constant. By using an AGC or limiter, it is seen that the performance of the PLL will improve inversely with the signal strength.

Table 1

Values of γ for Various Choices of Preprocessing Filter

PREPROCESSING FILTER	γ
$h(t) = \sin(2\pi t/T_s)$ $\quad 0 \leq t \leq T_s$ $0 \quad$ elsehwhere	3.58
$H(\omega) = j\omega \quad \lvert\omega\rvert \leq \omega_s$ $0 \quad$ elsewhere	6.97
$H(\omega) = j\omega\exp(-\omega^2/\omega_s^2)$	3.70

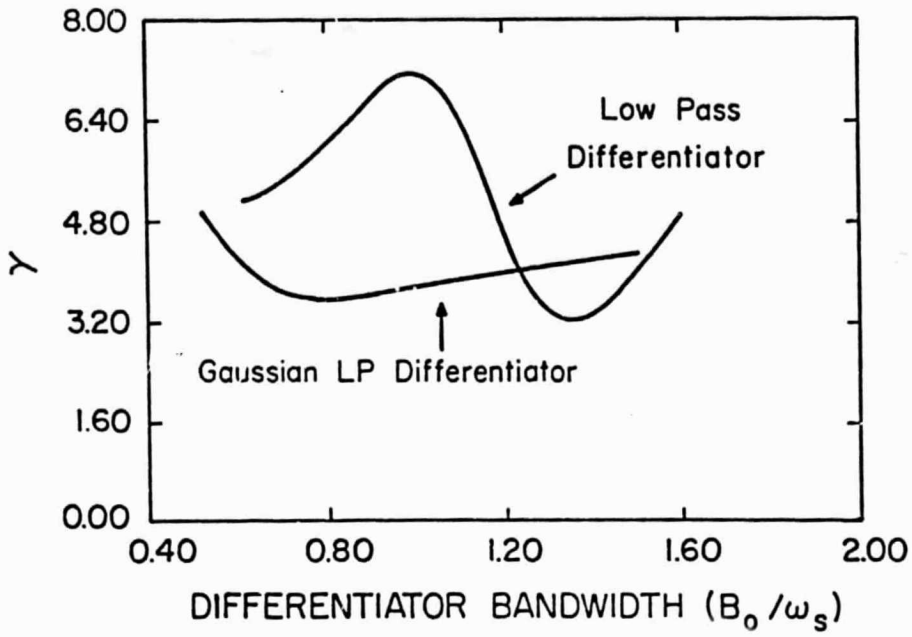

Figure 4. The value of γ as a function of the differentiator bandwidth for PPM systems with square transmitted pulses of width T_s. $H(\omega)$ is modeled as an ideal low pass differentiator, where B_0 is the cutoff frequency, and as a Gaussian low pass filter, where B_0 is the RMS bandwidth, followed by a differentiator.

5. COMPUTER SIMULATION

As was shown in the previous section, the timing reference generated by the PLL synchronizing circuit is in general a random variable with variance σ_ϕ^2, which is inversely proportional to the signal photocount, and is proportional to the order of PPM and the loop bandwidth.

In order to verify the expression of the variance of the phase error, a computer simulation of the phase-locked loop was developed. First, the output of the photodetector was generated as a Poisson arrival process with the count rate given by Equation (3). This photodetector output was then filtered and squared to simulate the effect of the preprocessing circuit. The output of the preprocessing circuit was then fed to the phase-locked loop simulator written in Advanced Continuous Simulation Language (ACSL) running on a CYBER-175. The simulator, modeled after the PLL in Figure 1, had the characteristics listed in Table 2.

Several simulations were carried out for different signal levels, each for a time period equal to 10,000 time slots, with the effective loop bandwidth, B_L, held constant for each simulation by adjusting the photodetector gain. The simulator calculated and recorded the phase error at the voltage controlled oscillator at the beginning of each time slot. The phase error variance of the VCO was then calculated from the simulated data. The results of the simulation are shown in Figures 5 through 7.

Figure 5a shows the power spectrum of the photodetector output before preprocessing. Notice the absence of the spectral peak at the slot frequency.

Table 2

Characteristics of the PLL Simulator

Normalized Signal Amplitude	$A = \frac{1}{2}$
Loop Filter	$F(s) = \frac{1}{20s + 1}$
VCO Gain Constant	$K_v = 0.33,\ 0.04$
Loop Bandwidth	$\frac{B_L}{\omega_s} = \frac{1}{2} AK_v$
Photodetector Gain	$G^2 = \frac{\pi T_w}{\lambda_s^2} \frac{1}{\lvert p(\omega)H(\omega) * p(\omega)H(\omega) \rvert}_{\omega = \omega_s}$
Preprocessing Filter	$h(t) = \begin{cases} \sin \frac{2\pi}{T_s} t & 0 \leq t \leq T_s \\ 0 & \text{elsewhere} \end{cases}$
Background Signal Level	$K_B = 0$

Figure 5b shows the spectrum of the preprocessed signal in which the spectral component at the slot frequency is clearly seen. Figures 6 and 7 contain plots of the variance of the phase error versus the signal count rate and the PPM order, respectively. The results show that the variance of phase error is proportional to the order of the PPM and is inversely proportional to the signal count rate. These results are in general agreement with Equation (34).

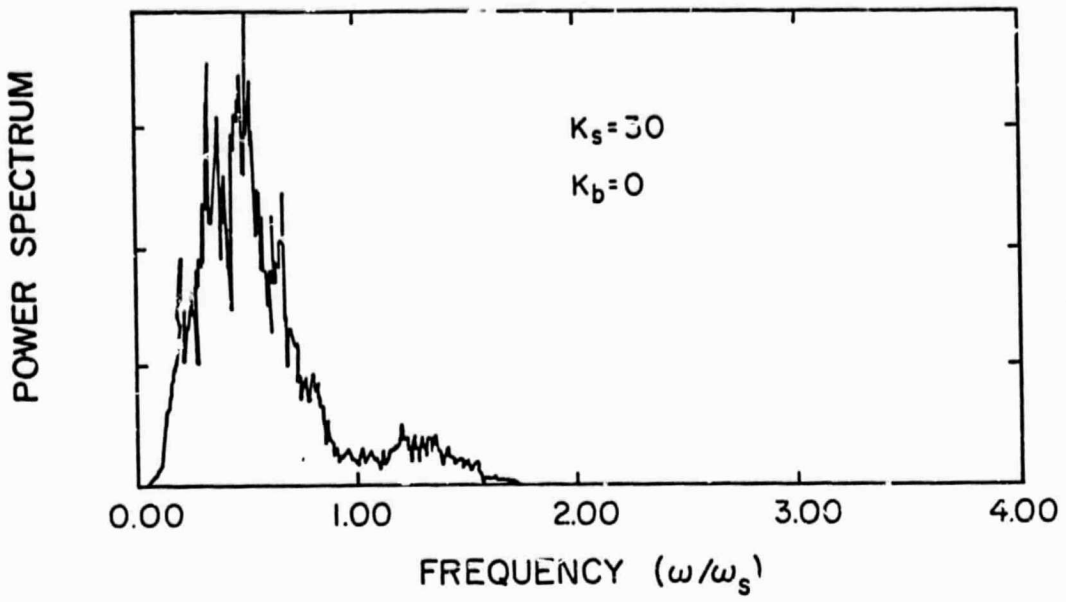

Figure 5a. Power spectrum of the simulated photodetector output for a 4-ary PPM system which transmits square pulses occupying the entire signal slot. No spectral peak is present at the slot frequency.

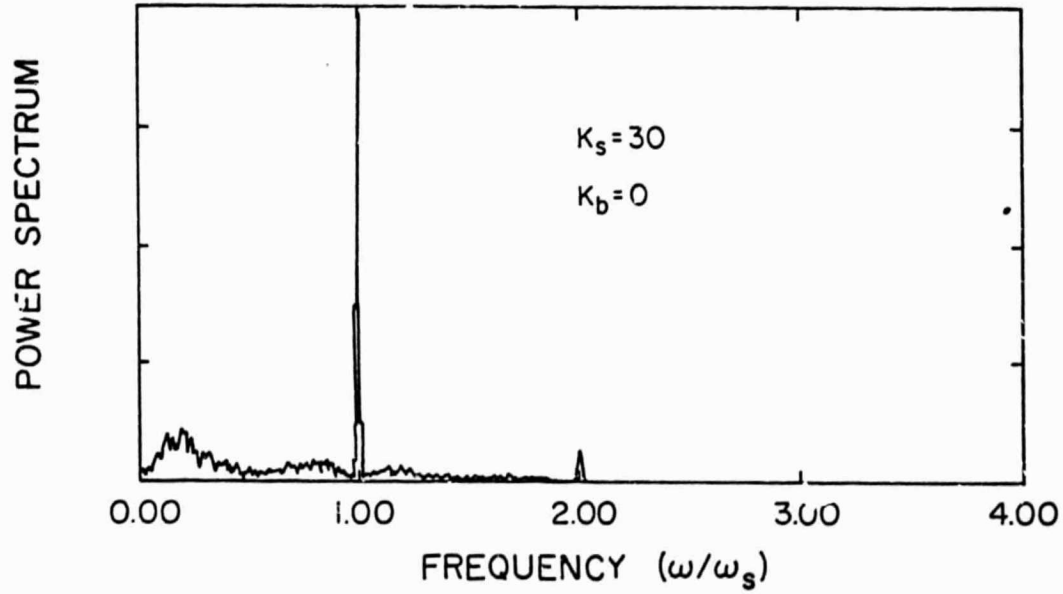

Figure 5b. Power spectrum of the preprocessed simulated photodetector output. A spectral peak at the slot frequency is clearly evident. The preprocessing filter impulse response h(t) used in this simulation was

$$h(t) = \begin{cases} \sin(\omega_s t) & 0 < t < T_s, \\ 0 & \text{elsewhere.} \end{cases}$$

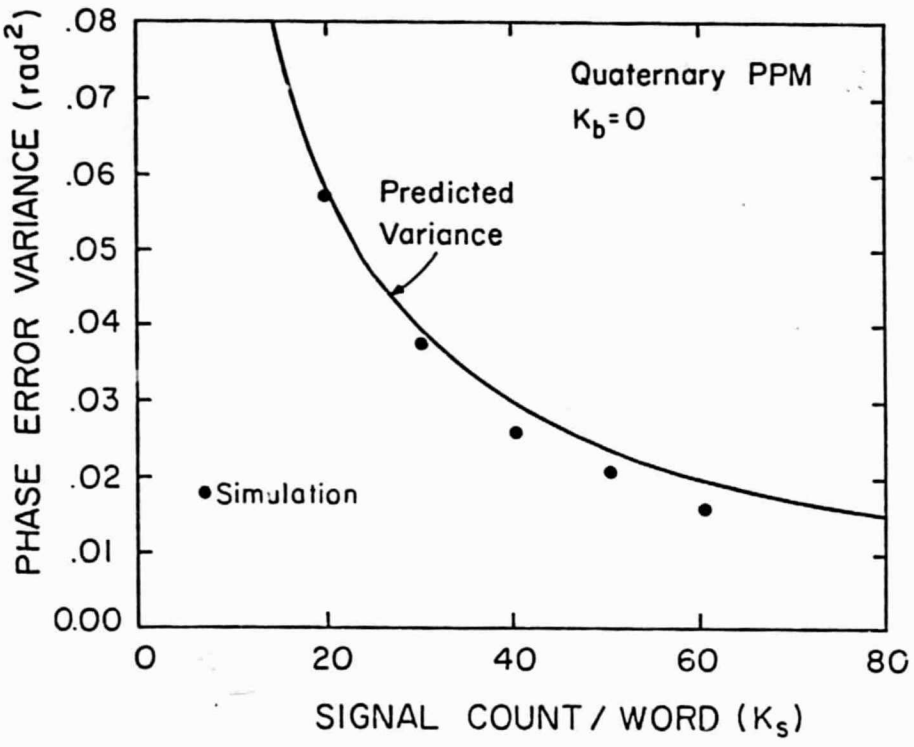

Figure 6. Computer simulated phase error variance versus the signal count rate for a 4-ary PPM receiver. The loop bandwidth and the order of the PPM are held constant during the simulation, and the VCO gain constant K_v is set to 0.33. The solid curve is the theoretical variance predicted by Equation (34).

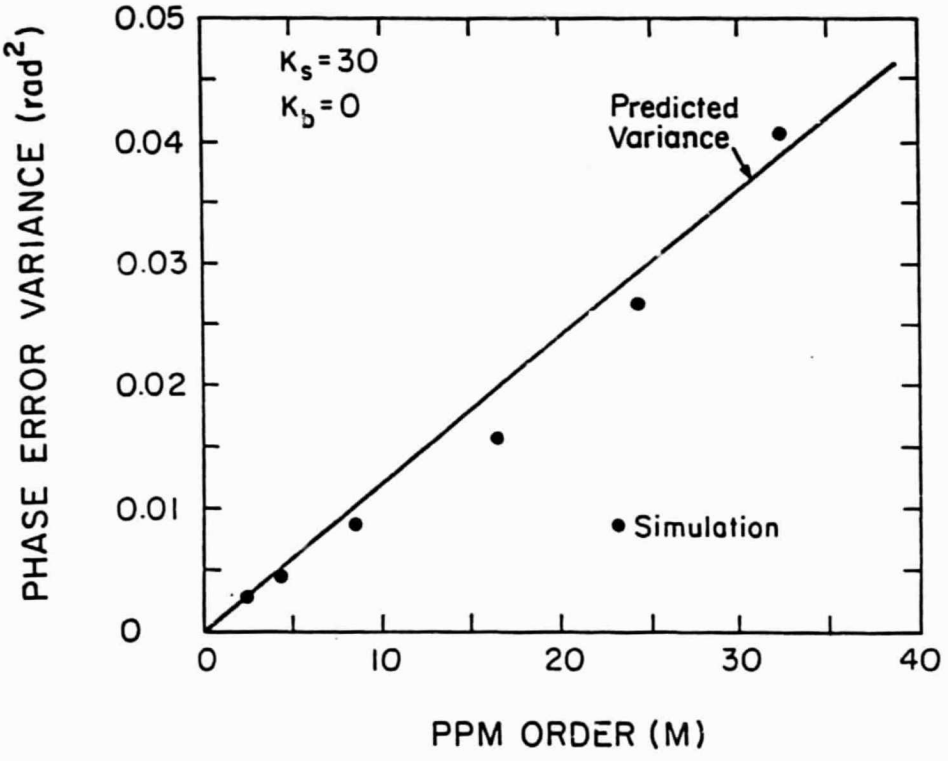

Figure 7. Computer simulated phase error variance versus the order of PPM for an M-ary PPM receiver. The loop bandwidth is held constant during the simulation by adjusting the gain of the preprocessing filter, and K_v is set to 0.04. The resulting phase error variance is proportional to the order of the PPM. The data points are the results of the simulation, and the solid line is the theoretical variance predicted by Equation (34).

6. PERFORMANCE OF PLL SYNCHRONIZED M-ARY PPM SYSTEM

The probability of word error (PWE) of a perfectly synchronized, shot noise limited M-ary PPM receiver using a photon counting detector has been shown to be [1,2]

$$PWE(K_s,K_b,M) = 1 - \frac{1}{M}e^{-(K_s + MK_b)} - \{\sum_{k=1}^{\infty} \frac{1}{k!}(K_s + K_b)^k \cdot e^{-(K_s + K_b)}$$

$$x\ [\sum_{\ell=0}^{k-1} \frac{K_b^{\ell}}{\ell!} e^{-K_b}]^{M-1}(\frac{(1 + a)^M - 1}{M \cdot a})\}$$

$$a \equiv \frac{K_b^K}{k!} \frac{1}{\sum_{\ell=0}^{k-1} \frac{(K_b^{\ell})}{\ell!}} \tag{35}$$

where $K_s = \lambda_s T_s$ and $K_b = \lambda_b T_s$ are the expected photocounts per slot due to the signal and background radiation respectively. The PWE given in Equation (35) is difficult to evaluate because of the large number of summations. For PPM systems with a large signal-to-noise ratio, the union bound can be used to give a good approximation of the PWE,

$$PWE(K_s,K_b,M) < (M-1) \cdot PWE(K_s,K_b,2) \quad . \tag{36}$$

$PWE(K_s,K_b,2)$ is the PWE of the binary PPM system, which is given by [14]

$$PWE(K_s,K_b,2) \triangleq \frac{1}{2}\left(1 + Q(\sqrt{2K_b}, \sqrt{2K_s}) - Q(\sqrt{2K_s}, \sqrt{2K_b})\right) \tag{37}$$

where $Q(\alpha,\beta)$ is Marcum's Q function, defined by

$$Q(\alpha,\beta) = \int_{\beta}^{\infty} e^{-(\alpha^2 + x^2)/2}\ I_0(\alpha x) \cdot x dx \quad . \tag{38}$$

The union bound of the PWE for a 4-ary PPM system is plotted along with the exact error rate evaluated by Equation (35) in Figure 8. The result shows an excellent agreement for large signal levels.

In the presence of receiver timing error, signal photons that are transmitted during the signal interval may be counted in the adjacent background slots, thereby increasing the probability of decoding error. For a fixed timing offset ΔT at the receiver, the expression for the PWE is very complicated and difficult to evaulate. However, if the amount of timing error is small, the union bound can again be used to approximate the PWE. Since the effects of the fixed timing error are to decrease the expected photocount in the signal slot and to increase the expected photocount in one of the two adjacent slots, we can write

$$PWE(K_s,K_b,M;\varepsilon) = PWE(K_s',K_b',2) + (M-2)PWE(K_s',K_b,2) \tag{39}$$

where we have expressed the timing offset ΔT in terms of the normalized timing error $\varepsilon = \Delta T/T_s$, and $K_s' = [(1-\varepsilon)\lambda_s + \lambda_b]T_s$ and $K_b' = (\varepsilon\lambda_s + \lambda_b)T_s$ are expected counts in the signal and affected adjacent slots, respectively. The first term on the right-hand side of Equation (39) is the error rate of the binary PPM system consisting of the signal time slot and the "contaminated" background slot, and the second term is the error rate of the (M-2) binary PPM systems composed of the signal slot and one of the remaining background slots. Figure 9 is a plot of the PWE of a 4-ary PPM system versus the fixed timing error, ε. The degradation of PWE with increasing ε is clearly seen.

Equation (39) gives an upper bound for PWE in the presence of a fixed timing error. For receivers employing dynamic phase synchronization circuits such as

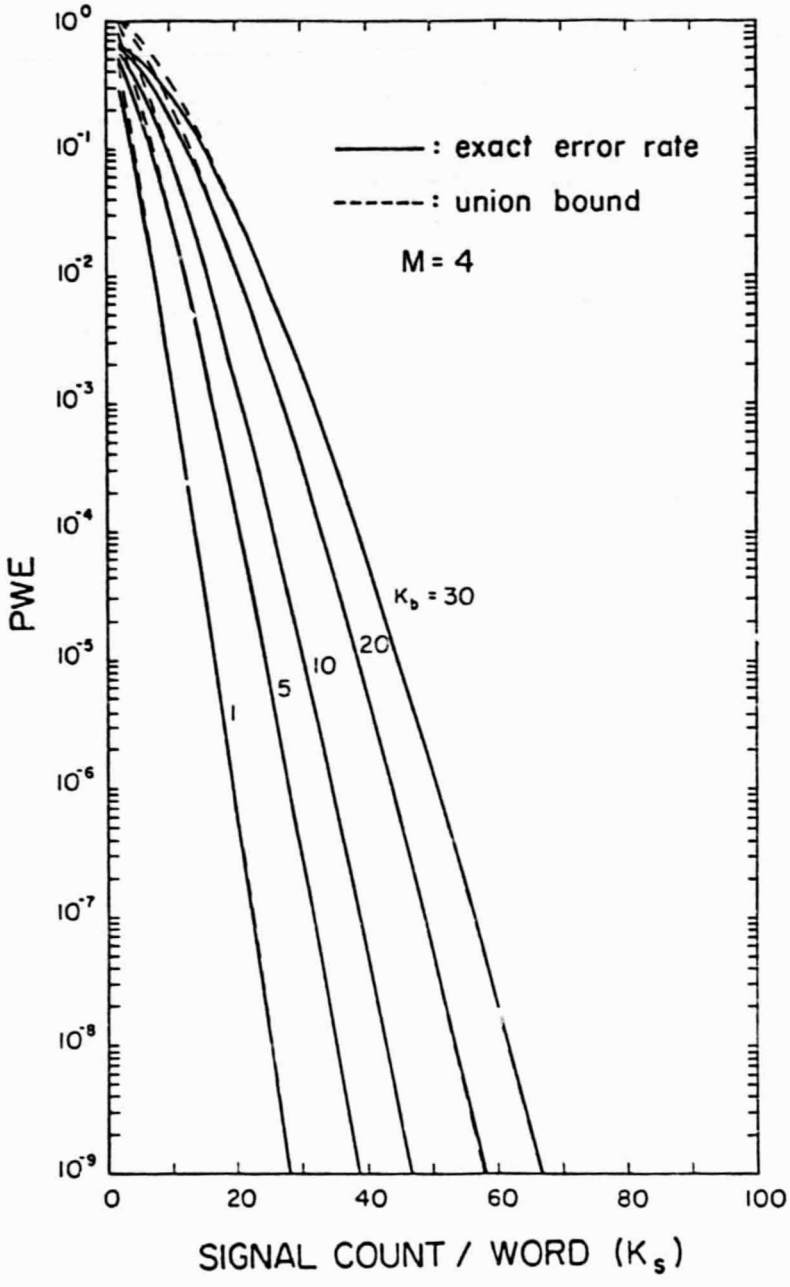

Figure 8. Comparison of the exact error rate and the union bound estimate for a 4-ary PFM system. Broken curves are the union bound given by Equation (36) and solid curves are the exact error rate given by Equation (35).

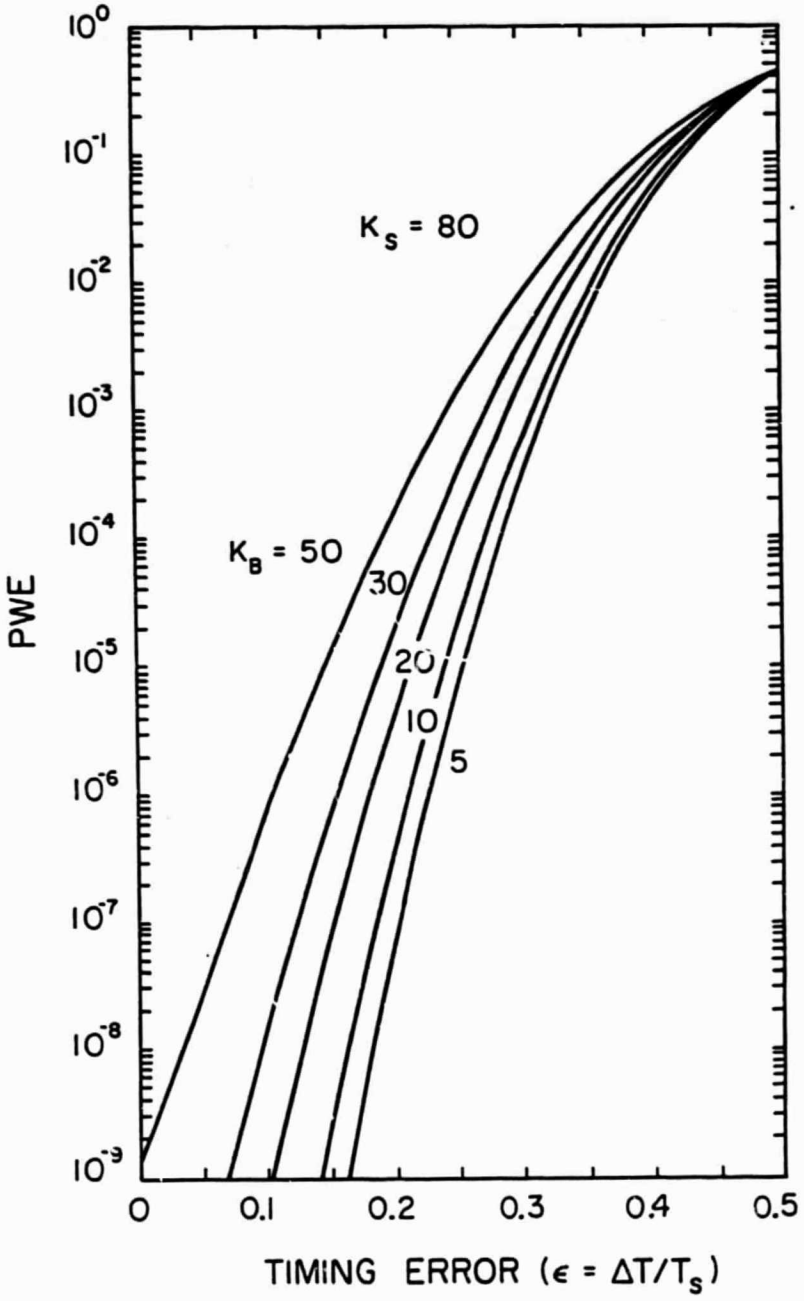

Figure 9. Probability of word error (PWE) of a 4-ary PPM receiver as a function of a fixed receiver timing error $\epsilon = \Delta T/T_S$, $K_S = 80$.

a PLL, the receiver timing error would in general be random. The exact probability distribution of the timing error is complicated to derive. From Equation (24), it is seen that the exact distribution of the timing error depends on the detailed statistical properties of the noise. However, when the loop bandwidth is small compared to the word frequency, the phase error can be regarded as a weighed average of the noise $\nu(t)$, given in Equation (26), over many periods of the transmitted word. Because $\nu(t)$ is essentially uncorrelated over different transmitted words, it is seen that the probability distribution of the timing error will be approximately Gaussian. A similar problem was studied by Gagliardi and Haney [6], in which they show that the phase distribution for a PLL driven by a shot noise limited synchronization channel was given by

$$P_{\phi}(\phi) = \frac{\exp[\alpha\cos\phi]}{2\pi I_0(\alpha)} \quad , \quad |\phi| < \pi \tag{40}$$

where I_0 is the modified Bessel function of order zero, and α is the average number of sync-signal counts occurring in the time period $1/2B_L$. For a well-synchronized system, ϕ is small, and P_{ϕ} can again be approximated by a Gaussian.

For a PLL synchronized system, the timing error remains essentially constant over a given word because the loop bandwidth B_L is usually much smaller than the word frequency. The unconditioned error probability for such a system is therefore the expectation of Equation (39) with respect to the distribution of ε, which is approximately Gaussian,

$$PWE(K_s,K_b,M) = \frac{1}{\sqrt{2\pi}\sigma_{\varepsilon}} \int_{-\infty}^{\infty} PWE(K_s,K_b,M,\varepsilon)e^{-\varepsilon^2/2\sigma_{\varepsilon}^2}\, de \tag{41}$$

Equation (41) is difficult to evaluate in a closed form. In general, numerical integration is required. Figure 10 is a plot of the PWE versus the expected signal count, K_s, for a 4-ary PPM system in which the receiver timing error is assumed to be Gaussian distributed. The result shows a severe degradation of receiver performance with increasing timing error variance.

The timing error variance σ_ε^2 for a PLL synchronized M-ary PPM system can be related to the phase error variance σ_ϕ^2 derived in the previous section by

$$\sigma_\varepsilon^2 = \sigma_\phi^2/(2\pi)^2 = \frac{1}{(2\pi)^2}\frac{\gamma M B_L}{K_s \omega_s} = \frac{\langle \Delta T^2 \rangle}{T_s^2} \tag{42}$$

Combining (41) and (42), the PWE of a PLL synchronized PPM system can now be expressed as a function of K_s, K_b, M, B_L, and γ. The effect of these parameters on the performance of the PLL synchronized PPM system can then be studied and compared to the perfectly synchronized system.

When comparing the performance of different communication systems, it is usually desirable to express the error probability in terms of the probability of bit error (PBE). For M-ary PPM, the PBE is related to the PWE by

$$\text{PBE} = \frac{1}{2}\left(\frac{M}{M-1}\right) \cdot \text{PWE} \quad . \tag{43}$$

Numerical evaluation of PBE has been carried out for various signaling conditions and receiver loop bandwidths. The results are shown in Figures 11 through 14. Figure 11 is a plot of the PBE versus signal count for various loop bandwidths. It is seen that for small loop bandwidths ($B_L/\omega_s < 10^{-3}$), the performance of the PLL synchronized system is almost identical to that of the perfectly

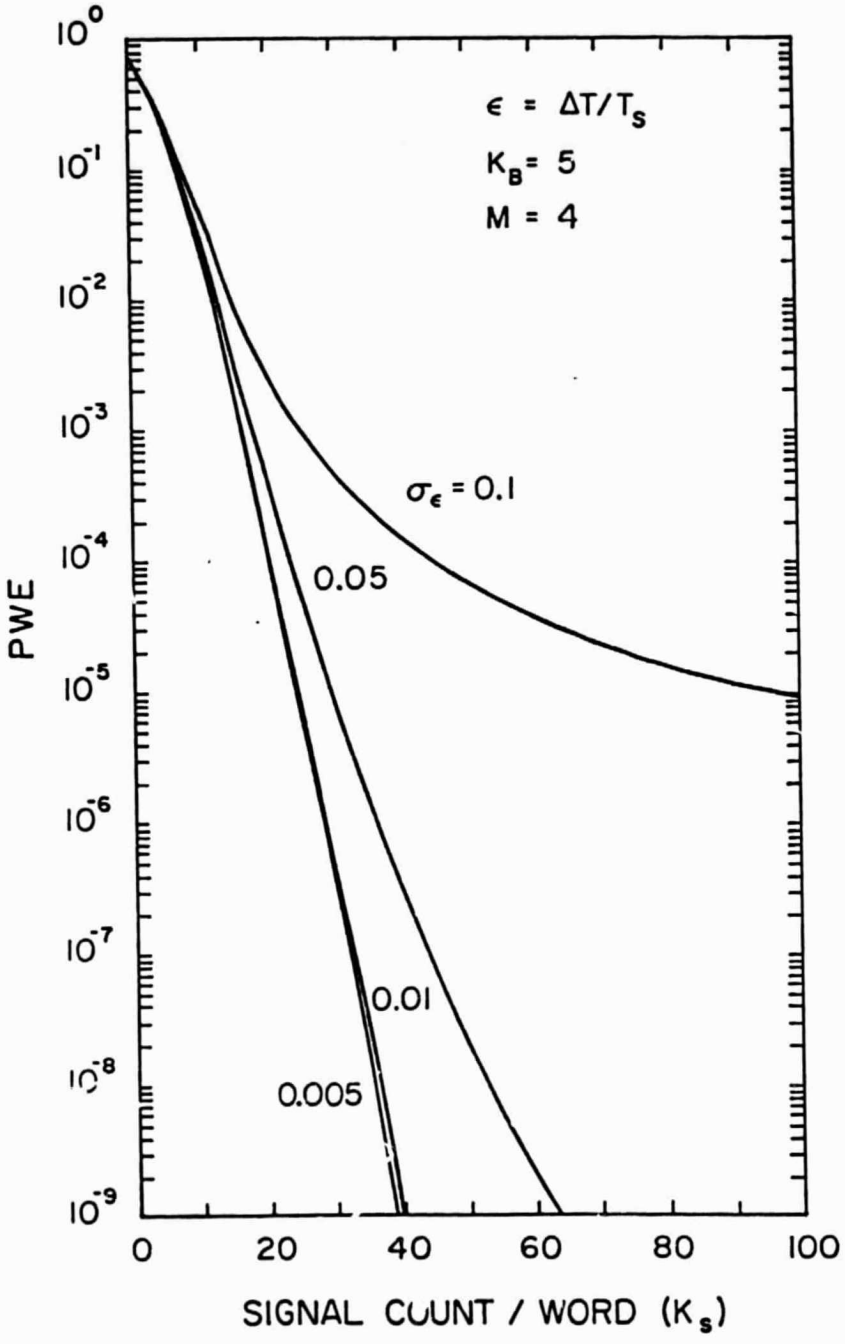

Figure .0. Probability of word error (PWE) of a 4-ary PPM receiver as a function of K_s, the expected signal photocount per word, for different values of the receiver timing error variance. The timing error is assumed to be Gaussian distributed. Background count rate $K_b = 5$.

synchronized system. For large loop bandwidths ($B_L/\omega_s > 10^{-2}$), however, higher signal levels are needed to compensate for the effects of synchronization errors. Figure 12 is a plot of the PBE versus signal count for various background noise levels and loop bandwidths. Again, it is seen that when the loop bandwidth is sufficiently small ($B_L/\omega_s < 10^{-3}$), only small increases in signal power are needed to achieve the same performance as the perfectly synchronized system. The increases in signal power needed to compensate for the imperfect synchronization can be described in terms of a system loss factor. Figure 13 is a plot of the loss factor versus the loop bandwidth at a fixed PBE of 10^{-9} for a 4-ary and a 8-ary PPM system. It is seen that for small loop bandwidths ($B_L/\omega_s < 10^{-3}$), the imperfect synchronization accounts for only 0.1 decibel loss in system performance, while at higher loop bandwidths ($B_L/\omega_s \approx 10^{-1}$), the loss can be significant.

The effect of increasing PPM order on the performance of the PPM system was also studied. The PBE of a perfectly synchronized PPM system decreases with increasing PPM order. For PPL synchronized PPM systems, however, the variation of PBE with PPM order is more complicated, because the timing error is also a function of the PPM order. Figure 14 is a plot of the PBE versus PPM order for various loop bandwidths and background count rates with the number of signal photons per bit and the equivalent bit period kept constant. It shows that for small loop bandwidths ($B_L/\omega_s \approx 10^{-4}$), the performance of the PLL synchronized PPM system is almost indistinguishable from the perfectly synchronized system at low PPM orders ($M < 10$). At higher PPM orders, however, because the phase error variance increases with PPM order, the degradation in performance will become

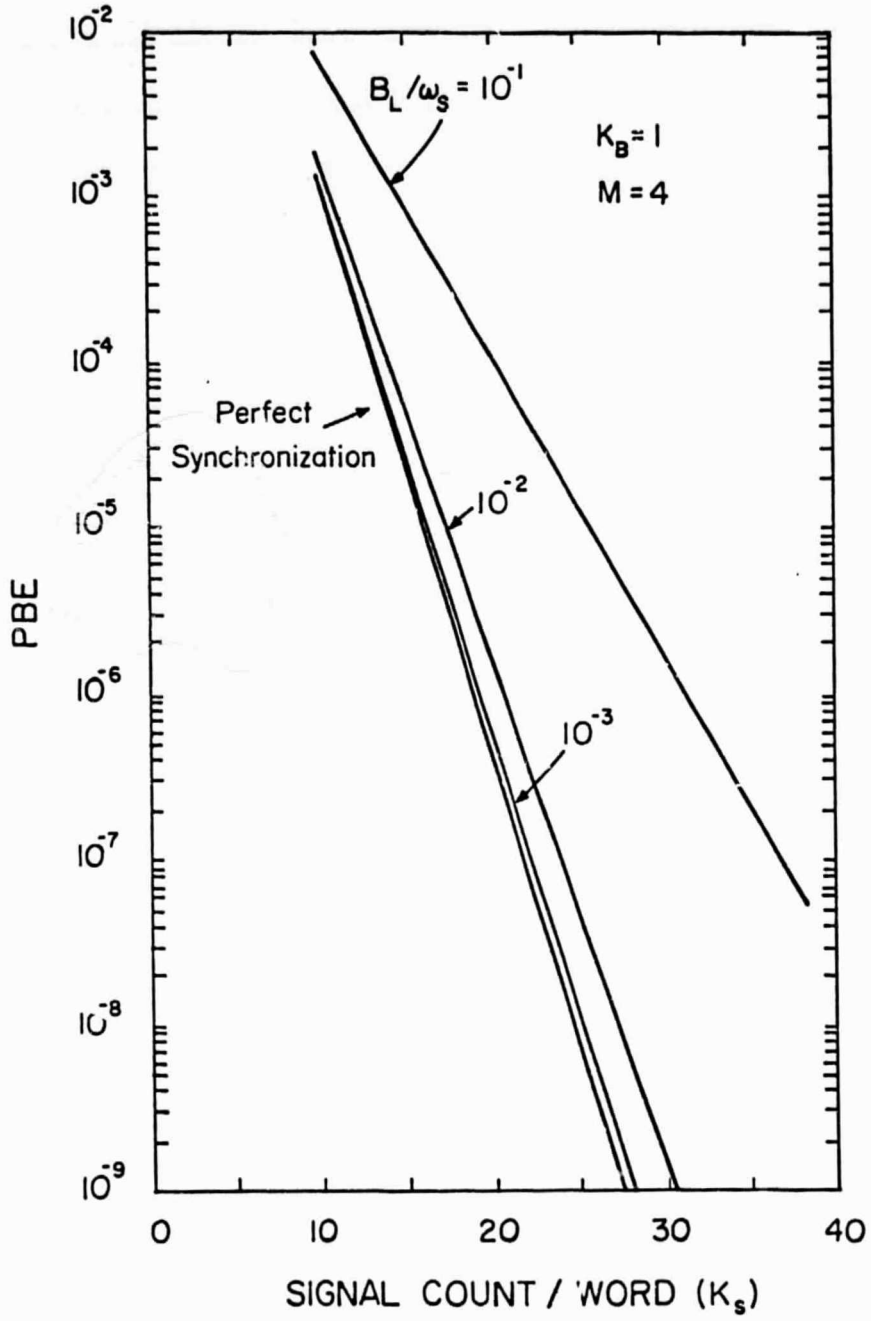

Figure 11. Probability of bit error (PBE) of a PLL synchronized 4-ary PPM system versus signal count/word for various loop bandwidths. $\gamma = 10$, $K_b = 1$.

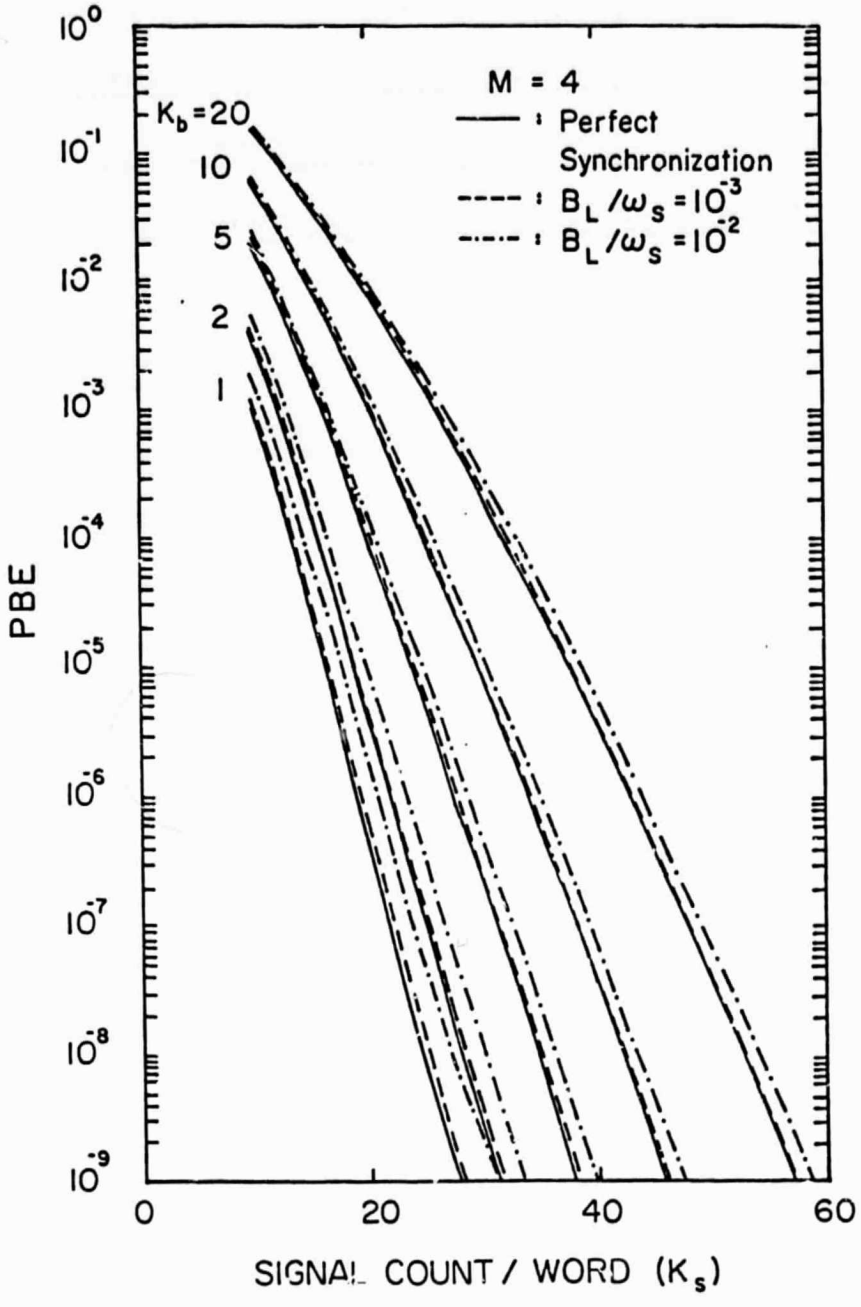

Figure 12. Probability of bit error (PBE) of a PLL synchronized 4-ary PPM system versus signal count/word for various background levels and bandwidths. $\gamma = 10$.

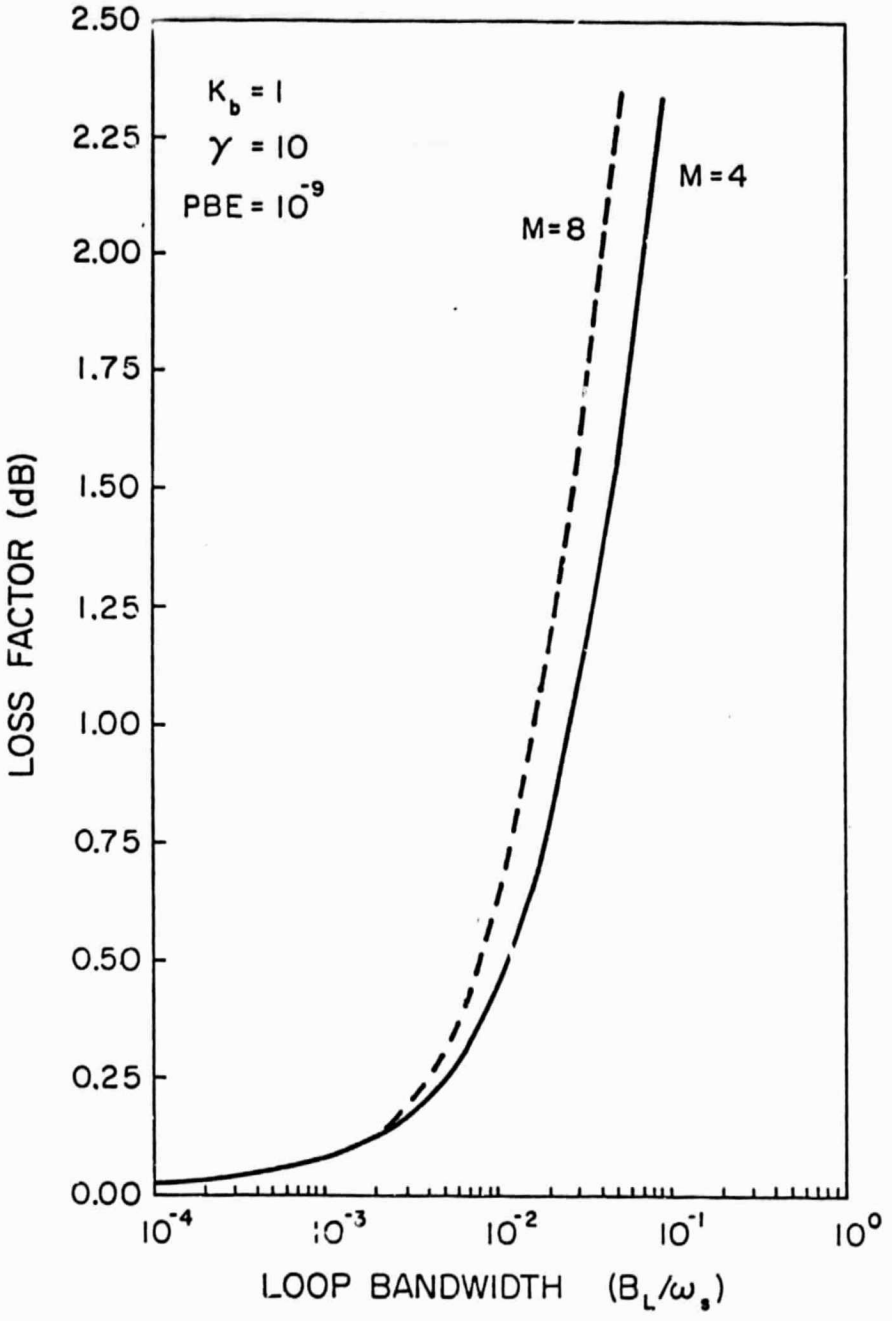

Figure 13. dB loss of transmitter energy versus the loop bandwidth for a PLL synchronized PPM system at PBE = 10^{-9} • $K_b = 1$, $\gamma = 10$.

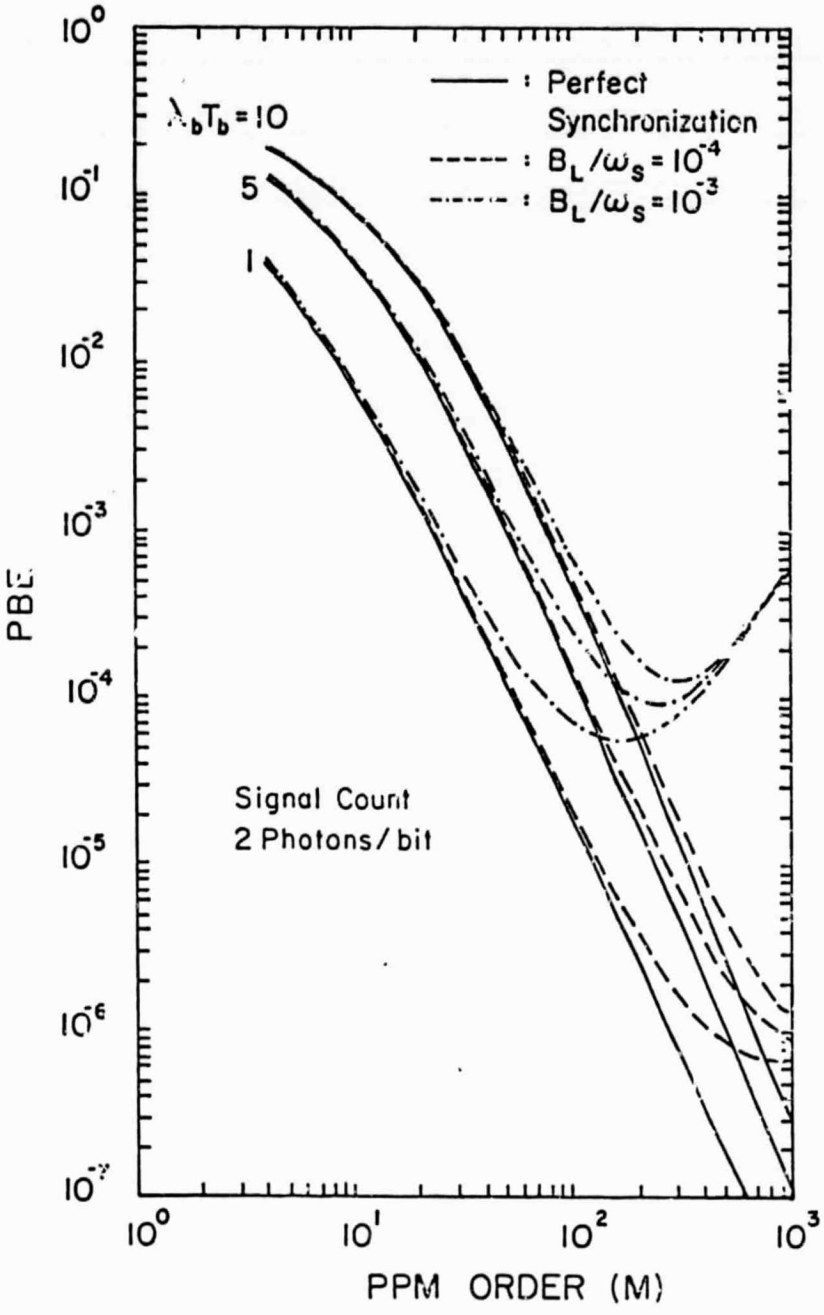

Figure 14. Probability of bit error (PBE) of a PLL synchronized PPM system versus the order of PPM for various background levels and loop bandwidths. The signal photon count per bit is fixed at 2, and the bit interval is kept fixed. $\gamma = 10$.

more apparent. In addition, since the synchronization error increases with PPM order, it is expected that the PBE will become an increasing function of PPM order at higher order PPM. Consequently, an optimal order of PPM exists that will minimize the PBE. Figure 14 shows that for a PPM system operating with a received signal level of two photons per bit and a background count rate of one photon ber bit interval, the PBE is minimized at M ≃ 100.

7. CONCLUSION

Phase-locked loops can be used to synchronize slot timing for an optical PPM system by preprocessing the photodetector output. With a gain control circuit or limiter at the input to the PLL, the synchronization performance is shown to improve with increasing signal power and decreasing loop bandwidth. Equation (10) shows that the requirement for preprocessing can be removed if the transmitted pulse shape does not have a vanishing Fourier transform at the slot frequency. In which case the power spectrum of the detector output would contain a component at the slot frequency that can be tracked out by PLLs. However, the preprocessing approach is preferred since non-square pulses usually require higher transmitter bandwidths and higher peak powers for the same number of photons transmitted.

The performance of the PLL synchronized system was studied and compared to that for the perfectly synchronized system. It is seen that higher signal levels are necessary to compensate for the imperfect synchronization due to the PLL. However, the loss in signal power is less than 0.1 decibel for loop bandwidths less than 0.1% of the slot frequency. This relatively small loss suggests that phase-locked loop synchronization PPM systems can be used to achieve reliable communications at a small increase in signal power.

APPENDIX A: POWER SPECTRUM OF THE PHOTODETECTOR OUTPUT

The output of the photodetector can be modeled as a filtered Poisson process,

$$i(t) = \sum_{\{\tau_j\}} h(t - \tau_j) \tag{A.1}$$

where h(t) is the impulse response of the detector filter. In general, the output of the photodetector defined above is not a stationary process. In fact, it is known that for PPM signaling, the output of the photodetector is cyclostationary with period T_w, where T_w is the word period. Consequently, the power spectrum of the photodetector output cannot be defined as the Fourier transform of its autocorrelation function. Nevertheless, the power spectrum remains a useful concept when discussing the frequency response of the system. We shall therefore define the time-averaged power spectrum for a nonstationary process as [1,10]

$$S(\omega) = \lim_{T\to\infty} \frac{1}{2T} E[|I_T(\omega)^2|]$$

where

$$I_T(\omega) = \int_{-T}^{T} i(t)e^{-j\omega t}dt \quad . \tag{A.2}$$

Substituting the definition of $I_T(\omega)$ into $S(\omega)$, we can rewrite (A.2) as

$$S(\omega) = \lim_{T\to\infty} \frac{1}{2T} E[\int i(t)i(\tau)e^{-j\omega(t - \tau)}dtd\tau]$$

$$= \lim_{T\to\infty} \frac{1}{2T} E_\lambda[\int E[i(t)i(\tau)|\lambda]e^{-j\omega(t - \tau)}dtd\tau] \quad . \tag{A.3}$$

n taking the joint expectation of the photodetector output, we first take the expectation conditioned on the detector photocount rate $\lambda(t)$, and then remove

the condition by taking the expectation with respect to λ. The conditional expectation of the filter Poisson process can be derived by differentiating the joint characteristic function $\Phi(\omega_1,\omega_2)$, given by

$$\Phi(\omega_1,\omega_2) = \exp[\int \lambda(\xi)[e^{-j(\omega_1 h(t-\xi) + \omega_2 h(\tau-\xi)} - 1)d\xi] \quad .$$

The result is

$$E[i(t)i(\tau)|\lambda] = -\frac{\partial^2 \Phi}{\partial\omega_1 \partial\omega_2}\Big|_{\omega_1 = \omega_2 = 0}$$

$$= \int \lambda(\xi)h(t-\xi)h(\tau-\xi)d\xi + \int\lambda(\xi)\lambda(\eta)h(t-\xi)h(\tau-\eta)d\xi d\eta \quad . \tag{A.4}$$

By substituting Equation (A.4) into (A.3) and carrying out the Fourier transform, the power spectrum of the photodetector output can be written as

$$S(\omega) = \lim_{T\to\infty} \frac{1}{2T} |H(\omega)|^2 E[\Lambda_T(0) + |\Lambda(\omega)|^2] \tag{A.5}$$

where $\Lambda_T(\omega) = \int_{-T}^{T} \lambda(t)e^{-j\omega t}dt$ is the Fourier transform of the received photocount rate. For the PPM signaling scheme, $\Lambda_T(\omega)$ is given by

$$\Lambda_T(\omega) = 2T(\frac{\sin\omega T}{\omega T})\ \lambda_b + \lambda_s\ p(\omega) \sum_k e^{-j\omega(kT_w + C_k T_s)} \tag{A.6}$$

where λ_s, λ_b, and C_k's are defined in Equation (3), and $P(\omega)$ is the Fourier transform of the pulse shape p(t). The expectation in Equation (A.5) is now taken with respect to the information sequence C_k. Using the sum rule $\sum_{i,j} = \sum_{i=j} + \sum_{i\neq j}$ and the fact that C_k's are indepenaent for nonoverlapping codewords, the expectation in Equation (A.6) can be evaluated. The resulting power spectrum is

$$S(\omega) = |H(\omega)|^2 \cdot \{(\lambda_b + \frac{\lambda_s}{M}) + 2\pi\delta(\omega)(\lambda_b^2 + \frac{2\lambda_s\lambda_b}{M}) + \frac{\lambda_s^2}{T_w} |p(\omega)|^2(1 - |R(\omega)|^2)$$

$$+ \frac{2\pi}{T_w} \lambda_s^2 \cdot |p(\omega)|^2 \sum_k \delta(\omega - 2\pi k/T_s)\} \qquad (A.7)$$

where

$$R(\omega) = E[e^{-jC_k\omega T_s}] = \frac{1}{M} \sum_{\ell=0}^{M-1} e^{-j\ell\omega T_s} \qquad (A.8)$$

and we have used the fact that

$$\lim_{T\to\infty} 2T \left(\frac{\sin\omega T}{\omega T}\right) = 2\pi\delta(\omega) \quad . \qquad (A.9)$$

APPENDIX B: POWER SPECTRUM OF THE PREPROCESSED SIGNAL

The output of the signal preprocessing circuit is the square of the filtered Poisson process

$$i_2(t) = \left(\sum h(t - \tau_j)\right)^2 \tag{B.1}$$

where h(t) is the combined impulse response of the preprocessing filter and the photodetector response function.

By substituting Equation (B.1) into (A.3) and taking the expectation of the filtered Poisson process, the power spectrum of the preprocesed signal can be written as

$$\begin{aligned} S(\omega) = \lim_{T\to\infty} \frac{1}{2T} E_\lambda\Big[\int e^{-j\omega(t-\tau)} \Big\{ \int \lambda(x)h^2(t-x)h^2(\tau-x)dx \\ + \left(\lambda(t)*h^2(t)\right)\left(\lambda(\tau)*h^2(\tau)\right) + \int \lambda(x)\lambda(y)h(t-x)h(t-y)h(\tau-x)h(\tau-y)dxdy \\ + 2\left(\lambda(t)*h^2(t)\right)\int \lambda(x)h(t-x)h^2(\tau-x)dx + 2\left(\lambda(\tau)*h(\tau)\right)\int \lambda(y)h(\tau-y)h^2(t-y)dy \\ + 4\left(\lambda(t)*h(t)\right)\left(\lambda(\tau)*h(\tau)\right)\int \lambda(x)h(t-x)h(\tau-x)dx + \left(\lambda(t)*h^2(t)\right)\left(\lambda(\tau)*h(\tau)\right)^2 \\ + \left(\lambda(\tau)*h^2(\tau)\right)\left(\lambda(t)*h(t)\right)^2 + \left(\lambda(t)*h(t)\right)^2\left(\lambda(\tau)*h(\tau)\right)^2\Big\}dtd\tau\Big] \quad . \end{aligned} \tag{B.2}$$

Here the expectation is taken with respect to the photocount rate $\lambda(t)$. Inspection of Equation (B.2) shows the complexity of the power spectrum. Notice that only terms involving λ^4 and λ^3 are significant, since all terms will be negligible in the limit of a large photocount. Equation (B.2) can therefore be simplified by dropping terms corresponding to lower order λ's. Carrying out the Fourier transform on the remaining terms, the power spectrum can be written as

$$S(\omega) = \lim_{T\to\infty} \frac{1}{2T} E[2\Lambda_T(\omega)H_2(\omega) \cdot (\Lambda_T(\omega)H(\omega)*\Lambda_T(\omega)H(\omega))*$$

$$+ 2\Lambda_T^*(\omega)H_2^*(\omega)(\Lambda_T(\omega)H(\omega)*\Lambda_T(\omega)H(\omega))$$

$$+ 4 \int \Lambda_T(\omega')\Lambda_T^*(\omega'')\Lambda_T^*(\omega' - \omega'')H(\omega')H(\omega - \omega')H^*(\omega'')H^*(\omega - \omega'')d\omega'd\omega''$$

$$+ |\Lambda_T(\omega)H(\omega)*\Lambda_T(\omega)H(\omega)|^2]$$

where

$$H_2(\omega) = \int h^2(t)e^{-j\omega t}dt \quad . \tag{B.3}$$

The expectation is now taken with respect to $\Lambda_T(\omega)$, the Fourier transform of the photocount rate. By substituting Equation (A.6) into Equation (B.3) and taking the expectation of the variables C_k's, the power spectrum of the preprocessed signal can be obtained. This power spectrum is very complicated and further simplifications are needed. First, it is assumed that the preprocessing filter blocks the dc component of the signal, which is due largely to the uniform background count rate and contains no timing information. Next, note that after taking the expectation with respect to C_k, the expression of the power spectrum contains integrals of the following form

$$I = \int |R(\omega')|^2 \cdot G(\omega')d\omega' \tag{B.4}$$

where $R(\omega)$ is given by (A.7), and $G(\omega')$ is some function of H and P, the Fourier transforms of h(t) and p(t). A plot of the function $R(\omega)$ shows that the magnitude of R is appreciable only in the vicinity of $\omega = 2\pi k/T_s$. Therefore, if the function $G(\omega)$ is slowly varying over the region where R is appreciable, we may

approximate the function $|R(\omega)|^2$ under the integral sign by a train of delta functions,

$$|R(\omega)|^2 \approx \frac{2\pi}{T_w} \sum_k \delta(\omega - 2\pi k/T_s) \tag{B.5}$$

where $T_w/2\pi = \int_0^{2\pi/T_s} |R(\omega)|^2 \, d\omega$ is the area under each peak of $|R(\omega)|^2$. The width of each peak of $|R(\omega)|^2$ is the order of ω_s/M, where M is the order of the PPM and $\omega_s = 2\pi/T_s$ is the slot frequency. For most cases of interest, $H(\omega)$ and $P(\omega)$ are slowly varying with respect to R such that the approximations holds. Finally, since $\lambda_s >> \lambda_b$ for most cases of interest, only terms involving λ_s^3 and λ_s^4 in the power spectrum will be retained.

With these assumptions, the power spectrum of the photodetector output can be approximated. The result, after lengthy calculation, is given by

$$S(\omega) = \frac{1}{2\pi} \cdot \frac{\lambda_s^4}{T_w^2} |P(\omega)H(\omega) * P(\omega)H(\omega)|^2 \cdot \sum_k \delta(\omega - 2\pi k/T_s)$$

$$+ \frac{4}{(2\pi)^2} \frac{\lambda_s^3}{T_w} \int P(\omega')P^*(\omega'')P^*(\omega' - \omega'')H(\omega')H(\omega - \omega')H^*(\omega'')H^*(\omega - \omega'')d\omega' d\omega'' \; . \tag{B.6}$$

REFERENCES

[1] R. Gagliardi and S. Karp, "M-ary Poisson Detection and Optical Communications," IEEE Trans. Commun. Technol., Vol. CT-17, No. 2, Apr. 1969, pp. 208.

[2] S. Karp and R. Gagliardi, "The Design of PPM Optical Communication Systems," IEEE Trans. Commun. Technol., Vol. CT-17, Dec. 1969, pp. 670.

[3] R. Gagliardi, "The Effect of Timing Errors in Optical Digital Systems," IEEE Trans. Commun. Technol., Vol. CT-20, No. 2, Apr. 1972.

[4] W. C. Lindsey, Synchronization Systems in Communcation and Control. Englewood Cliff, NJ: Prentice-Hall, 1973.

[5] A. J. Viterbi, Principles of Coherent Communcations. New York: McGraw-Hill, 1966.

[6] R. Gagliardi and M. Haney, "Optical Synchronization Phase-Locking with Shot Noise Process," USCEE Report 396, Aug. 1970.

[7] R. H. Forrester and D. L. Snyder, "Phase Tracking Performance of Direct-Detection Optical Receivers," IEEE Trans. Commun., Vol. COM-21, pp. 1037-1039, Sept. 1973.

[8] U. Mengali, "Tracking Properties of Phase Locked Loops in Optical Communication Systems," IEEE Trans. Commun., Vol. COM-28, No. 9, Sept. 1978.

[9] C. N. Georghiades, "Joint Baud and Frame Synchronization in Direct Detection Optical Communications," IEEE Trans. Commun., Vol. COM-33, pp. 357-361, Apr. 1985.

[10] C. N. Georghiades and D. L. Snyder, "Locating data frames in direct detection optical communication systems," IEEE Trans. Commun., Vol. COM-32, pp. 118-123, Feb. 1984.

[11] S. D. Personick, "Receiver Design for Digital Fiber Optic Communication Systems, I," Bell Syst. Tech. J., Vol. 52, July 1973, pp. 843.

[12] D. L. Snyder, Random Point Processes. New York: Wiley, 1975.

[13] W. A. Gardner adn L. E. Franks, "Characterization of Cyclo-Stationary Random Signal Processes," IEEE Trans. Inform. Theory, IT-21, January 1975.

[14] W. K. Pratt, Laser Communications Systems. New York: John Wiley and Sons, 1969.

CUMULATIVE LIST OF RADIO RESEARCH LABORATORY
AND ELECTRO-OPTIC SYSTEMS LABORATORY REPORTS
PREPARED UNDER NASA GRANT NSG-5049

RRL Rep. No. 469 - Gardner, C. S. and N. N. Rao (December 1975), The Effects of Random Path Fluctuations on the Accuracy of Laser Ranging Systems.

RRL Rep. No. 471 - Zanter, D. L., C. S. Gardner and N. N. Rao (January 1976), The Effects of Atmospheric Refraction on The Accuracy of Laser Ranging Systems.

RRL Rep. No. 477 - Gardner, C. S. and J. R. Rowlett (November 1976), Atmospheric Refraction Errors in Laser Ranging Data.

RRL Rep. No. 478 - Hendrickson, B. E. and C. S. Gardner (December 1976), Correction of Laser Ranging Data for the Effects of Horizontal Refractivity Gradients.

RRL Rep. No. 481 - Gardner, C. S. (February 1977), Statistics of the Residual Refraction Errors in Laser Ranging Data.

RRL Rep. No. 486 - Gardner, C. S. (July 1977), Comparison Between the Refraction Error Covariance Model and Ray Tracing.

RRL Rep. No. 488 - Gardner, C. S. (September 1977), Speckle Noise in Satellite Based Lidar Systems.

RRL Rep. No. 495 - Gardner, C. S. and G. S. Mecherle (April 1978), Speckle Noise in Direct-Detection Lidar Systems.

RRL Rep. No. 496 - Gardner, C. S. and A. M. Saleh (October 1978), Speckle Noise in Differential Absorption Lidar Systems.

RRL Rep. No. 499 - Gardner, C. S. (January 1979), A Technique for Remotely Measuring Surface Pressure from a Satellite Using a Multicolor Laser Ranging System.

RRL Rep. No. 502 - Palluch, E., J. D. Shelton and C. S. Gardner (May 1979), Operating Manual for the RRL 8 Channel Data Logger.

RRL Rep. No. 505 - Gardner, C. S. and R. Axford, Jr. (March 1980), Regression Models for Multicolor Satellite Laser Ranging.

RRL Rep. No. 510 - Gardner, C. S. (April 1981), Analysis of Target Signatures for Laser Altimeters.

RRL Rep. No. 511 - Gardner, C. S. (June 1981), Atmospheric Refraction Effects in Air Borne Laser Ranging.

RRL Rep. No. 514 - Tsai, B. and C. S. Gardner (December 1981), Remote Sensing of Sea State by Laser Altimeters

RRL Rep. No. 518 - Gardner, C. S. (August 1982), Optical Communications.

RRL Rep. No. 519 - Im, K. E. and C. S. Gardner (September 1982), Atmospheric Refraction Effects on Baseline Error in Satellite Laser Ranging Systems.

RRL Rep. No. 526 - Im, K. E., B. M. Tsai and C. S. Gardner (September 1983), Analysis of Short Pulse Laser Altimetry Data Obtained Over Horizontal Path.

RRL Rep. No. 527 - Tsai, B. M. and C. S. Gardner (March 1984), Theoretical and Experimental Analysis of Laser Altimeters for Barometric Measurements Over the Ocean.

EOSL Rep. No. 84-001 - Lafaw, D. A. and C. S. Gardner (August 1984), Timing Performance of Phase-Locked Loops in Optical Pulse Position Modulation Communication Systems.

EOSL Rep. No. 85-002 - Im, K. E. and C. S. Gardner (April 1985), Estimation of the Differential Pulse Propagation Times in Two-Color Laser Ranging Systems.

EOSL Rep. No. 85-003 - Chen, C. C. and C. S. Gardner (May 1985), Phase-Locked Loop Synchronization for Direct Detection Optical PPM Communication Systems.